sustainability

MDPI

Article

Sensing System for Cooking Event Detection Designed to Control Indoor Air Quality

Monika Maciejewska [1], Jan Szecówka [2], Paulina Dziurska [1] and Andrzej Szczurek [1,*]

[1] Faculty of Environmental Engineering, Wroclaw University of Science and Technology, 50-370 Wrocław, Poland; monika.maciejewska@pwr.edu.pl (M.M.); paulinadziurska@gmail.com (P.D.)
[2] Technical Academy of Informatics in Applied Sciences, 54-239 Wrocław, Poland
* Correspondence: andrzej.szczurek@pwr.edu.pl

Abstract

Giving consideration to cooking activity is important for sustainable housing. In contexts of limited ventilation, imposed by energy saving concerns, cooking causes deterioration of indoor air quality (IAQ) and occupants' discomfort. This study presents a cooking event detection system that may support IAQ control to minimize the impact of cooking. The system consists of a multi-sensor device and a deep-learning neural network (DNN). The device monitors temperature (T), relative humidity (RH), suspended particulate matter (PM), CO_2, the responses of sensors to volatile organic compounds (VOCs), and other gases (NO_2, CO, CH_2O) in the kitchen zone. The collected data are processed by the DNN. The detection system generates a response every 7 s, indicating either 'COOKING' or 'NO COOKING'. Feature vector selection was based on classification performance and cost considerations. Cooking event misdetections generate unjustified IAQ control costs: economic ones (UEC), when the system detects a non-existent event, and environmental ones (UEN), when the system fails to detect an actual event. In this study, several well-performing detection systems were developed, with miss rates ranging from 5.1% to 20.5% and false detection rates ranging from 7.7% to 11.7%. The results show that gas sensor responses—particularly to VOCs—had greater utility for cooking event detection compared with T, RH, CO_2, and PM. The cost analysis demonstrated that IAQ control supported by the developed cooking event detection systems could generate higher total unjustified environmental costs when the unit cost ratio UEN/UEC exceeded 1.25, or higher total unjustified economic costs when the unit cost ratio UEN/UEC was below 1.43. We believe this work will contribute to the development of novel automatic IAQ control systems supported by event detection.

Keywords: indoor air quality; cooking event; deep learning neural network; sensor device; cost analysis

Check for updates

Academic Editor: Giouli Mihalakakou

Received: 12 December 2025
Revised: 20 January 2026
Accepted: 9 February 2026
Published: 12 February 2026

1. Introduction

In recent years, the concept of sustainable development has been extensively debated [1]. Sustainability in the building sector refers to the design, construction, and operation of structures in a manner that is environmentally responsible and resource-efficient throughout their entire life cycle [2]. Sustainability is attained by using green materials, conserving energy and water, reducing waste, and integrating built environments with natural systems, while simultaneously accounting for economic and social considerations. Sustainable development promotes healthy living environments. However, the question of how to ensure high indoor air quality, thermal comfort, and access to natural light—while giving respect to sustainability principles remains a matter of ongoing discussion due to differing viewpoints [3,4].

A major challenge in sustainable housing is the inherent tension between reducing energy consumption and maintaining adequate quality of indoor environment, in particular, indoor air quality. Energy consumption in buildings is a critical issue, and in efforts to reduce it, buildings are increasingly constructed to be airtight [5]. While airtightness improves energy efficiency and reduces greenhouse gas emissions, it can adversely affect indoor air quality [6]. Pollutants may originate from various everyday sources, including cleaning products, furniture, building materials, and occupant activities such as, e.g., cooking [7,8].

The supply of outdoor air is a key factor in improving indoor air quality. Ventilation helps remove or dilute airborne pollutants generated indoors. Contaminant concentrations indoors are reduced and overall indoor air quality (IAQ) is improved. Natural ventilation, which relies on outdoor airflows to refresh indoor spaces, can be energy-efficient and beneficial for IAQ. However, it is not always feasible or effective due to climatic or site conditions [9]. Mechanical ventilation systems provide greater control over supply airflow and pollutants removal but they consume energy and require ongoing maintenance. Sustainable ventilation strategies therefore aim to balance natural and mechanical ventilation. Oftentimes, incorporation of energy-recovery technologies and smart control systems allows to minimize energy use while ensuring sufficient fresh air supply and effective pollutant removal [10].

Giving consideration to cooking activity is important for sustainable housing. Cooking and food preparation are basic human activities that influence the quality of the indoor environment, particularly the air quality [8]. Cooking is accompanied by heat generation, the emission of water vapor, chemical species [11], particulate matter [12], as well as various sounds [13]. These factors may adversely affect human health [14,15]. Moreover, the cooking fumes - associated discomfort experienced by occupants has recently become an increasingly important issue, especially in multi-family buildings. Most people, who are exposed to high workload and stress, have high expectations regarding conditions at home, perceived as their primary place of rest. Earlier research has recognized that the restorative effect of home environments depends on interior characteristics, e.g., sound, lighting, greenery, window view, furnishing materials and forms [16–19]. Due to a recent shift toward working from home, the influence of indoor conditions on employee performance became another extensively studied problem [20].

Cooking emissions may induce an adverse hedonic effect (unpleasant odor), ultimately giving rise to stench pollution [21]. A nuisance may result from the persistence of the species released in the kitchen and their transport throughout the flat, or even the entire building [22]. The full decay time of PM2.5 generated during cooking was estimated at 1 to 10 h for the kitchen and living room [12]. Occupants may also suffer from cross-contamination throughout the building due to shared kitchen exhaust ducts. Approximately two interunit kitchen exhaust transmission events per day were identified during a 2-month monitoring campaign in a representative multilevel residential building [23]. These transmissions increased occupants' exposure to particulate matter (PM), black carbon (BC), NOx, CO, and volatile organic compounds (VOCs) in both the kitchen and the living room.

The impact of cooking on indoor air quality can be controlled. The most common IAQ control measures (IAQCM) include kitchen windows, stove hoods, exhaust fans, and portable air cleaners (PAC). Their positive effects have been confirmed experimentally. Intervention strategies, including opening kitchen windows and using PACs either in the kitchen or the living room, substantially lowered indoor PM2.5 levels and shortened the full decay time [12]. An advanced IAQ control strategy (automated stove hood, portable air cleaners, and bathroom exhaust) allowed PM2.5 concentration to be reduced by 40% in the flat and by 20% in the kitchen, compared with a standard strategy (ventilation and a manually operated stove hood) in a typical U.S. home [24]. However, despite the increasing availability of IAQCM, manually controlled devices are usually not used effectively. The reasons include energy costs, maintenance issues (e.g., filter replacement), noisy operation, or the cook's distraction [21]. Implementing automatic control in IAQCM could potentially enable more effective management of cooking-related IAQ impacts [25].

Home cooking is typically neither continuous nor long-lasting. It has been reported that, in residential apartment buildings, people usually cook for 20–30 min, amounting to only a few percent of the daytime [26]. The impact of cooking on the indoor environment may be considered an event. An event may be defined as an activity planned for a specific purpose, usually producing characteristic consequences, such as a change of state. It may occur uniquely or repeatedly. A cooking event may be defined as the preparation of food for human consumption occurring at a specific time and place. Detecting cooking events is critical for enabling automatic control of their impact on IAQ.

The problem of cooking event detection has been addressed in several studies. The proposed approaches typically include two components: the collection of data indicative of cooking occurrence, and a classifier that recognizes the data patterns characteristic of such events. Various types of data have been considered. For example, sound recognition technology has been applied to cooking detection. Based on a limited set of sound data, a convolutional neural network achieved an F1-score exceeding 80% [13]. Specific cooking activities were also recognizable based on associated sounds [27], e.g., frame-by-frame detection of grill cutting (F1-score of about 70%) [28]. A novel concept was to detect cooking activity using surface temperature and humidity signals of residential buildings via an LSTM autoencoder, achieving a precision of 66% and a recall of 85% [26]. Since cooking produces various emissions, its occurrence changes many indoor air parameters. For example, NO has been found indicative of cooking events in kitchens [11]. Numerous studies have shown that the mixture of VOCs in the air reflects a wide range of food types, preparation processes, and cooking styles. For example, alkanes were indicative of "home cooking" and "Hunan cuisine," whereas alkenes were characteristic of "Shandong cuisine" and "Barbecue" [21]. It was found that different chemical classes of VOCs were emitted depending on the unit operation: aldehydes during oil heating, monoterpenes during spice frying, and alcohols during the addition of vegetables [29]. Also a set of versatile indoor air parameters may provide an effective basis for cooking event detection. A recall of 75.5% and a precision of 52.66% were obtained with a neural network operating on data including indoor air temperature, relative humidity, PM2.5, total VOCs (TVOC), CO_2, CO, air pressure, O_3, and NO_2 concentration [30].

This work focuses on the development of a cooking event detection system. The system is designed to continuously monitor cooking occurrence and respond with "COOKING" or "NO COOKING" every few seconds, allowing for close to real time IAQ control. The case of cooking was chosen to illustrate the more general concept of IAQ control based on detection of indoor activities as opposed to utilizing IAQ assessment based on the responses of the individual sensors.

The essence of the approach proposed in this paper lies in the assumption that air quality can be associated with specific indoor activities. Practice shows that this assumption is fully justified. Individual activities affect the chemical state of indoor air, which in turn interacts with a matrix composed of multiple sensors that respond differently to the environment. It can therefore be assumed that air quality is reflected in the responses of these devices. Data analysis makes it possible to determine their relationship. Cooking

https://doi.org/10.3390/su18041910

events are assumed to be a proxy for poor indoor air quality, and if cooking is detected, then air quality control can be automatically activated.

The cooking event detection system, presented in this work uses indoor air parameter measurements and a deep learning neural network. The measurement data are collected by a multisensor device dedicated to indoor air monitoring, which may operate as an element of the Internet of Things [31].

The paper is structured as follows. Section 2 describes the cooking event detection system. Section 2.1 presents the multisensor device for indoor air quality monitoring; Section 2.2 outlines the deep learning neural network used as the classifier; Section 2.3 discusses feature vector construction; and Section 2.4 focuses on the evaluation approach for classification performance and the framework for analyzing unjustified economic and environmental IAQ control costs. Section 3 describes the measurement study. Section 4 presents the results and their analysis, including a) the importance of various air parameters and parameter groups in effective cooking event detection, and b) the evaluation of detection systems regarding classification performance and unjustified IAQ control costs. Section 5 provides the discussion, while Section 6 offers the summary and conclusions.

2. Materials and Methods

This work focuses on the detection of cooking events. The detection system is assumed to consist of a sensor device and a classifier. The sensor device measures selected indoor air parameters in the kitchen or kitchen zone, where these parameters are indicative of cooking activity. Measurements are performed continuously, with a predefined temporal resolution. The collected data, after appropriate preprocessing, are used by the classifier to identify cooking events. The detection system operates continuously and performs point-by-point detection. Each response refers to a single time point, whose duration is determined by the temporal resolution of the measurements obtained from the sensor device.

2.1. Sensor Device

The first component of the proposed cooking event detection system is a sensor device. In this work, a multi-sensor device was used to collect data on multiple indoor air parameters. Although currently commercial devices of this kind are already available and used [32] a prototype device was employed in our study (see Figure 1). It provides real-time measurements of a still wider range of physical and chemical quantities. They include temperature, relative humidity, pressure, CO_2 concentration, volatile organic compounds (including formaldehyde), NO_2, particulate matter, and light intensity.

The device features an innovative design and construction. Commercial low-cost sensors were utilized in a portable, compact, lightweight, energy-efficient, direct-reading instrument. The sensors cover a broad spectrum of measured parameters. They are arranged in individual sensing modules. For gas sensors, dynamic exposure was applied to ensure very short response times. The air flow through the gas sensor chamber is evoked by a miniature fan. The use of a miniature fan (0.5 W) instead of a vacuum pump allows for energy saving and quiet device operation. The gas chamber was specially designed to minimize flow resistance for fan use. The airflow through the sensor chamber protects the device from overheating during operation. The measurement characteristics of the sensors integrated into the device are shown in Table 1. The recommended/most reported values of target quantities were additionally provided to confirm the viability of the sensors used.

The device records data with a temporal resolution of 7 s. The MQTT protocol was used for data transmission and communication with the user. The instrument is capable of communicating with other devices as part of the Internet of Things. Its detailed characteristics have been presented elsewhere [31].

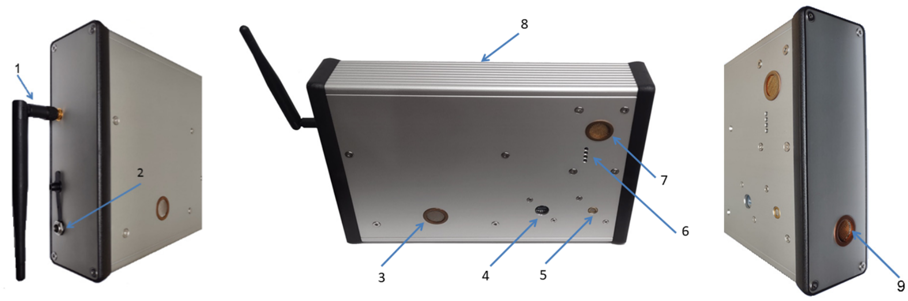

(**a**) (**b**) (**c**)

Figure 1. The multi-sensor device: (**a**) Side view (**b**) Front view. (**c**) Side view. The indicated elements:1—WiFi antenna, 2—power socket DC 5 V, 3—gas inlet for multi-cell sensing module, 4—light intensity sensor, 5—pressure sensor, 6—gas outlet for PM5003 sensor module, 7—gas inlet for the PM5003 sensor module, 8—aluminum housing, and 9—gas outlet for multi-cell sensing module. The size of the measurement device is 220 mm × 165 mm × 51.5 mm. Its weight is 1300 g. Reprinted from [31].

Table 1. Measurement characteristics of sensors integrated in the multi-sensor device, and the recommended/most reported values of target quantities in indoor air.

Sensor		Target	Measurement Accuracy	Measurement Range	Recommended Value
MPL3115A2 (NXP Semiconductors, Eindhoven, The Netherlands)		Pressure	0.1 kPa	50–110 kPa	Not available
BH1750 (OKYSTAR, Shenzhen, China)		Light intensity	1 lx	1–65,535 lx	300–500 lx in the kitchen [33]
TGS2600 (Figaro Engineering Inc., Osaka, Japan)		Hydrogen	Not available	1–30 ppm	Not available
TGS2602 (Figaro Engineering Inc., Osaka, Japan)		Ethanol	Not available	1–30 ppm	Not available (most reported TVOC < 1 mg/m^3) [34]
PID AH-2 (Alphasense, Great Notley, UK)		Isobutylene	Not available	1 ppb–50 ppm	Not available (most reported TVOC < 1 mg/m^3) [34]
Cozir-Blink5000 (Gas Sensing Solutions Ltd., Cumbernauld, UK)		Carbon dioxide	30 ppm	0–5000 ppm	<1000 ppm (8 h average) [35]
Grove Multichannel Gas Sensor V2 (Seed Technology Co Ltd., Shenzhen, China)	GM-102B	Nitrogen dioxide	Not available	0.1–10 ppm	200 µg/m^3 (1 h average) [36]
	GM-302B	Ethanol	Not available	1–500 ppm	Not available (most reported TVOC < 1 mg/m^3) [34]
	GM502B	Volatile organic compounds, ethanol	Not available	1–500 ppm	Not available (most reported TVOC < 1 mg/m^3) [34]
	GM702B	Carbon monoxide	Not available	5–5000 ppm	100 mg/m^3 (15 min average) [36]
PMS5003 (DFRobot, Shanghai, China)		Temperature	0.1 °C	−20 –99 °C	19–28 °C [37]
		Humidity	0.1%	0–99%	30–65% [38]
		Formaldehyde	0.01 mg/m^3	0–2 mg/m^3	100 µg/m^3 (30 min average) [36]
		Particulate matter (PM)	1 µg/m^3	0–500 µg/m^3	15 µg/m^3 (PM2.5) 45 µg/m^3 (PM10) (24 h average) [39]

An important stage of any measurement process is the calibration of the measuring instrument. This problem is particularly significant when the device is used to measure complex gas mixtures, as is the case in this study. The work focuses on the detection of episodes characterized by a specific air quality resulting from a complex mixture generated during a particular activity—cooking. It is difficult to define and subsequently prepare a gas that represents such an activity. Therefore, calibration of the developed instrument cannot be carried out using methods typically applied to gas detectors, monitors, or analyzers. In this study, the calibration problem was addressed using an alternative approach. The calibration data consisted of sensor responses recorded when the sensors were exposed to the gaseous environment present in the room during a specific activity. Because this environment could vary over time, the calibration data were obtained through multiple repeated exposures. In this way, a statistically valid reference pattern of sensor responses for a given activity was obtained. These patterns formed the basis for the calibration of the entire detection system, comprising the measuring device and the classifier.

2.2. Classifier

The second component of the cooking event detection system is a classifier. The classifier solves a two-class classification problem by assigning each feature vector to one of the following classes: 'COOKING' or 'NO COOKING'. Accordingly, the classifier may detect a cooking event (system output: 'COOKING') or detect the absence of such an event (system output: 'NO COOKING'). The system output is expected to correlate with the actual situation in the kitchen, i.e., to show 'COOKING' when a cooking event is taking place, and 'NO COOKING' when no such activity occurs.

A deep learning neural network (DNN) was applied as the classifier. A series of experiments was conducted using neural networks trained on several variants of input datasets. All variants shared a common neural network structure, preselected based on preliminary analysis. The network consisted of four fully connected hidden layers with 48, 36, 34, and 20 neurons, respectively. The Exponential Linear Unit (ELU) activation function was used for the hidden layers. The output layer consisted of a single neuron using a sigmoid transfer function. The number of input neurons depended on the particular variant of the input dataset.

Each neural network was trained for 50 epochs, with each epoch comprising approximately 190,000 iterations. Five-fold cross-validation was applied to evaluate network performance. For each dataset variant, training was repeated five times, starting from random initial weights and using a different subset of data for testing. The experiments were carried out using TensorFlow tools with Keras libraries in a Python 3.11 environment. All networks were trained with the *Adam* optimizer, using a learning rate of 0.001 and momentum factors of 0.9 (β_1) and 0.999 (β_2).

2.2.1. Neurons' Activation Functions

The ELU transfer function (see Figure 2a) was applied to the neurons in the hidden layers of the neural network. This function is based on the Rectified Linear Unit (ReLU) activation function which is defined by Equation (1).

$$f(x) = 0 \text{ for } x < 0, \text{ and } f(x) = x \text{ for } x > 0 \quad (1)$$

The advantages of ReLU in neural networks include computational simplicity (calculating the ReLU value requires only a single conditional operation in code), representational sparsity (ReLU outputs zero for negative inputs, allowing many neurons to remain completely inactive, which simplifies the network), and linear behavior (ReLU is linear for positive inputs, which facilitates training by mitigating the vanishing gradient problem).

https://doi.org/10.3390/su18041910

Despite these advantages, ReLU was rarely used for a long time because, from a formal mathematical perspective, it is not differentiable at zero (the threshold value, strictly speaking). The ELU function is a slightly more refined alternative (see Equation (2)).

$$f(x) = \exp(x) - 1 \text{ for } x < 0, \text{ and } f(x) = x \text{ for } x > 0 \quad (2)$$

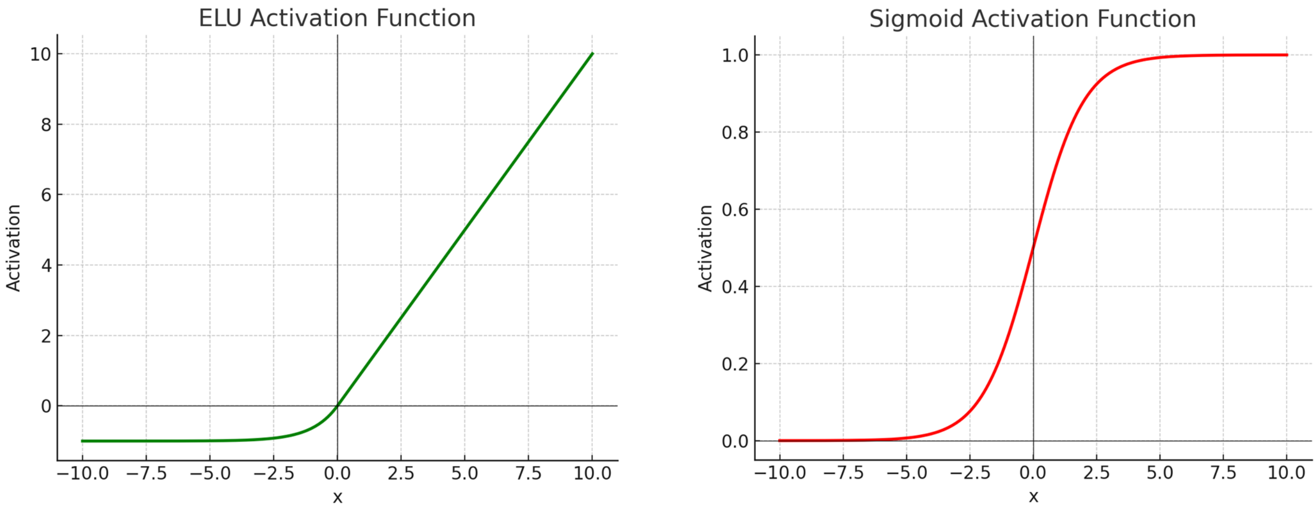

(**a**) (**b**)

Figure 2. Activation (transfer) functions applied in the DNN in this study. (**a**) ELU activation function, see Equation (2). It was applied to the neurons in the hidden layers of DNN. (**b**) Sigmoid activation function, see Equation (3). It was applied to the single neuron in the output layer.

Its shape is similar to ReLU, although it exhibits some characteristics of the sigmoid function. For negative inputs, it asymptotically approaches a constant value, and it is differentiable over the entire range. On the other hand, computing its derivative is more complex than for ReLU. In addition to producing unbounded positive outputs, ELU can also generate small negative values, which may enhance the local processing capabilities of the neuron layers.

A sigmoid activation function (see Figure 2b) was applied to the single neuron in the output layer of the neural network. This is a classic approach in neural networks, extensively used since the early development of the technology. It is defined by the formula in Equation (3).

$$f(x) = 1/(1 + e^{-x}) \quad (3)$$

The sigmoid function provides a combination of desirable properties: in the central part of its range, it behaves approximately linearly: it resembles a simple 0–1 switch, although it never reaches exactly zero or one, and it remains differentiable across its entire range.

2.2.2. Training Procedure

In the classic gradient-based method for neural network training [40], the modification of each weight w in the next iteration t is based on the partial derivative of the objective function $\partial Q/\partial w$, sometimes enhanced by the momentum term from the previous update $\Delta w(t-1)$ (Equation (5)). The relative influence of these two mechanisms is controlled by the coefficients α and β (Equations (4) and (5)).

$$w(t+1) = w(t) + \Delta w(t) \quad (4)$$

$$\Delta w(t) = -\alpha \frac{\partial Q}{\partial w}(t) + \beta \Delta w(t-1) \tag{5}$$

The Adam algorithm [41] is a significantly extended version of this method. In addition to the standard gradient (i.e., the vector of derivatives of the objective function with respect to all network weights), it also considers the squared gradient (i.e., the vector of squares of these derivatives). These two vectors are used to compute, at each iteration, two key components for updating the weights: the first moment estimator m and the second moment estimator v.

The first moment estimator (Equation (6)) is a weighted sum of the current gradient and its previous value, with the weights balanced by the parameter β_1 and its complement to 1. Similarly, the second moment estimator (Equation (7)) combines the square of the gradient with its previous value, adjusted by the parameter β_2. Both parameters take values in the interval [0, 1) and are usually fixed throughout the training process.

$$m(t) = \beta_1 \cdot m(t-1) + (1-\beta_1) \cdot \frac{\partial Q}{\partial w} \tag{6}$$

$$v(t) = \beta_2 \cdot v(t-1) + (1-\beta_2) \cdot \left(\frac{\partial Q}{\partial w}\right)^2 \tag{7}$$

Before being used to update the weights, each moment undergoes a bias correction (Equations (8) and (9)) to compensate for the effects of initializing with zeros at the beginning of training. Both formulas involve powers of β_1 and β_2, where the exponent corresponds to the iteration number. Since both parameters are fractions, raising them to higher powers causes the resulting values to approach zero, gradually reducing the effect of the correction mechanism. This ensures that moment correction is applied primarily during the initial phase of training.

$$\hat{m}(t) = \frac{m(t)}{1-\beta_1^t} \tag{8}$$

$$\hat{v}(t) = \frac{v(t)}{1-\beta_2^t} \tag{9}$$

Finally, the new weight is computed according to Equation (10), following the general iterative rule (Equation (4)). In Equation (10), an additional parameter ε, a small positive constant, is included to prevent division by zero, without affecting the underlying calculation.

$$\Delta w(t) = -\alpha \frac{\hat{m}(t)}{\sqrt{\hat{v}(t)} + \epsilon} \tag{10}$$

Adam is considered one of the most efficient optimization methods for neural network training. It typically converges much faster than the classic gradient descent method. A major advantage is its robustness when gradients are close to zero, which is particularly important in multilayer, deep neural networks. In such networks, the contribution of an individual weight to the overall error is small, leading to the vanishing gradient problem—a significant obstacle for classical learning methods. Therefore, Adam is a highly effective alternative for deep learning approaches derived from Geoffrey Hinton's framework [21], including the decomposition of large networks into Boltzmann machines with alternating forward and backward phases.

2.3. Rationale for Choosing DNN

In this work, we focused on a DNN network to have more strict control on how deep we reach into the history of samples, and this way, investigate how far the previous data is relevant. An obvious alternative, LSTM is a very powerful technique indeed, probably the highest achievement of the 20th Century in neural networks. Concerning time series processing, it has one disadvantage. The training process gathers the history of samples, but it is not clear how far it reaches into history, how quickly it forgets previous data. The process of resetting the long-term memory component is slow and fuzzy rather than sharp and instant. In our work, we applied sufficiently large DNN networks and fed them with several variants of input vector size, being different lengths of sample windows. This way, we gathered more explicit knowledge about static/dynamic features of the data, which we need for future work.

In this context, CNN networks, with a one-dimensional probe, would bring similar comparative knowledge (based on manipulation of probe size). We have some experiments behind us, although we found the results of the presented DNN solution more consistent.

It shall be additionally mentioned that we used the ADAM algorithm for training, which is classified among the highest achievements in feedforward network training. It can handle bigger networks in a quite efficient way. So, it was a kind of game changer, raising some interest as an alternative to (classic now) Geoffrey Hinton's approach to deep learning (decomposition to RBMs, forward/backward phases, etc.). It has also undermined the opinion on LSTM or CNN's explicit superiority over DNNs.

2.4. Feature Vector

The measurement data recorded by the multi-sensor device were used for cooking event detection. The data included the following air parameters: T, RH, CO_2, PM10, PM2.5, and PM1. They also included the responses of the following sensors: TGS2600, TGS2602, PID-AH, GM102b, GM302b, GM502b, GM702b, and PMS5003 (CH_2O). A measurement data vector consisted of the air parameters and sensor responses recorded at a single time point. Pre-processing was applied to prepare the data for the neural network, following several steps:

1. Combining the time series from all measurement days: The data were organized into a single multivariate time series.
2. Variable normalization: Min-max scaling to the range [0, 1] was applied to each variable.
3. Data annotation: Each measurement data vector was assigned a label. Vectors recorded during cooking (class 'COOKING') were labelled '0.9', while vectors recorded when no cooking occurred (class 'NO COOKING') were labelled '0.1'. Labels of 1 and 0 were avoided to ensure that the data remained within the approximately linear portion of the sigmoid activation function.
4. Feature vector construction and flag assignment: A feature vector consisted of data vectors from one or more consecutive time points. Sequences of 3, 5, 7, and 9 time points were used. Each feature vector was assigned the label of the most recent data vector included in it (as determined in step 3).
5. Preparation for five-fold cross-validation: The table of feature vectors was divided into two parts: vectors flagged '0.9' ('COOKING') and vectors flagged '0.1' ('NO COOKING'). The rows of each table were shuffled using a fixed random seed to ensure reproducibility. Each table was then divided into five equal parts. Each subset of vectors flagged '0.9' was combined with a different subset of vectors flagged '0.1', resulting in five sets of feature vectors. In each set, the relative representation of 'COOKING' and 'NO COOKING' patterns was preserved. The vectors representing the two categories were also randomly selected. These five datasets were used in the five-fold cross-validation procedure.
6. Dimensionality reduction: The sensor data were pruned to obtain smaller subsets, including only selected measured parameters. Three approaches were applied: (a) re-

moving a single measured parameter from the entire set, (b) removing an entire group of parameters based on predefined criteria (e.g., type of measured quantity, sensor manufacturing technology), and (c) retaining only a selected group of parameters based on the same criteria while eliminating all others.

2.5. Performance Evaluation of the Cooking Event Detection System

Table 2 presents the confusion matrix for the cooking event detection problem. True positives (TP) correspond to cases (time points) in which cooking actually occurred and was correctly detected by the system. False positives (FP) represent cases in which no cooking took place, but the system incorrectly detected a cooking event. False negatives (FN) correspond to cases in which cooking occurred but was not detected by the system. True negatives (TN) represent cases in which no cooking took place, and the system correctly indicated its absence.

Table 2. Confusion matrix for the cooking event detection problem.

		Detected	
		'COOKING' (PP)	**'NO COOKING' (PN)**
Occurred	'COOKING' (P)	TP	FN
	'NO COOKING' (N)	FP	TN

P—positive, N—negative, PP—predicted positive, PN—predicted negative, TP—true positives, FN—False negatives, FP—false positives, TN—true negatives.

Unjustified costs may arise when IAQ control is managed based on cooking event detection, due to the nonzero probability of misdetections. The unjustified environmental cost (UEN) occurs when a cooking event takes place (occurred: 'COOKING'), but the detection system fails to identify it (detected: 'NO COOKING'), as shown in Table 3. In this case, the IAQ control mechanism (IAQCM) does not operate despite being needed, resulting in a deterioration of indoor air quality and the associated UEN cost.

Table 3. Positioning of the unjustified costs of IAQ control associated with cooking event misdetection with reference to the confusion matrix shown in Table 2.

		Detected	
		'COOKING' (PP)	**'NO COOKING' (PN)**
Occurred	'COOKING' (P)	No unjustified cost	Unjustified environmental cost (UEN)
	'NO COOKING' (N)	Unjustified economic cost (UEC)	No unjustified cost

P—positive, N—negative, PP—predicted positive, PN—predicted negative.

Conversely, the unjustified economic cost (UEC) occurs when no cooking event takes place (occurred: 'NO COOKING'), but the detection system incorrectly signals a cooking event (detected: 'COOKING'). In this scenario, the IAQCM operates unnecessarily, leading to unwarranted consumption of materials and energy, which constitutes the UEC cost.

A comparison of Tables 2 and 3 highlights the relationship between cooking event misdetections and the corresponding unjustified costs of IAQ control. As shown, false negatives (FN) correspond to unjustified environmental costs, while false positives (FP) correspond to unjustified economic costs. Based on this correspondence, FP and FN were selected as the primary metrics for assessing classification performance in this work. They

https://doi.org/10.3390/su18041910

were also used to evaluate the detection system in terms of the unjustified costs associated with IAQ control.

2.5.1. Classification Performance: Miss Rate and False Detection Rate

The primary assessment of the cooking event detection system was based on classification performance, which was used to determine the optimal composition of the feature vector for the classifier. The Miss Rate (MR) and False Detection Rate (FDR) were applied as evaluation metrics. These metrics correspond to the conditional probabilities of false negative and false positive detections, respectively.

In general, the Miss Rate (MR) indicates the proportion of relevant items (P) that are not retrieved (FN), as defined in Equation (11).

$$\mathrm{MR} = \frac{\mathrm{FN}}{\mathrm{P}} = \frac{\mathrm{FN}}{\mathrm{TP} + \mathrm{FN}} \tag{11}$$

In this work, MR represents the fraction of actual cooking events (P) that remained undetected (FN). In other words, MR is the conditional probability of failing to detect a cooking event that actually occurred.

The False Detection Rate (FDR) indicates the proportion of retrieved items (PP) that are not relevant (FP), as defined in Equation (12).

$$\mathrm{FDR} = \frac{\mathrm{FP}}{\mathrm{PP}} = \frac{\mathrm{FP}}{\mathrm{TP} + \mathrm{FP}} \tag{12}$$

In this study, FDR represents the fraction of detected cooking events (PP) that did not actually occur (FP). That is, FDR is the conditional probability that a detected cooking event was a false alarm.

MR and FDR were selected as the primary classification performance measures to avoid reliance on true negatives (TN). Cooking event detection is a rare-event detection problem, where the dataset is typically unbalanced and contains fewer positively labelled samples than negatively labelled ones [12]. In our study, the measurement dataset representing the actual cooking events was much smaller than the dataset representing the absence of cooking. The percentage of cooking data vectors was 4.9%, while the percentage of no-cooking data vectors was 95.1%. This imbalance leads to a large number of true negatives. Including TN in performance evaluation in such cases can result in an overoptimistic assessment; therefore, MR and FDR were considered more appropriate metrics for this application.

2.5.2. Cost Aspect: Unjustified Environmental Cost and Unjustified Economic Cost of IAQ Control

An additional framework was proposed to evaluate the performance of the cooking event detection system in terms of the unjustified costs of IAQ control associated with possible misdetections. This framework is applicable provided that both FP and FN are nonzero.

The total unjustified environmental cost ($\mathrm{UEN_T}$) of IAQ control over a period of n time points is given by Equation (13).

$$\mathrm{UEN_T} = \mathrm{UEN_U} \cdot \mathrm{FN_p} \cdot \mathrm{n} \tag{13}$$

Here, $\mathrm{UEN_U}$ is the unit unjustified environmental cost, representing the cost incurred when the IAQ control measures fail to operate despite being needed to compensate for the impact of cooking on indoor air quality. This cost is defined for a single time point. $\mathrm{FN_p} = \mathrm{FN}/(\mathrm{P} + \mathrm{N})$ is the probability of failing to detect a cooking event that actually occurred at a single time point (see Table 2). Based on Equation (13), for a given unit cost UEN_U, the total unjustified environmental cost UEN_T may vary depending on the probability of misdetection of truly occurring cooking events (FN_p).

Similarly, the total unjustified economic cost UEC_T of IAQ control over a period of n time points is given by Equation (14).

$$UEC_T = UEC_U \cdot FP_p \cdot n \quad (14)$$

Here, UEC_U is the unit unjustified economic cost, representing the cost of operating the IAQ control measures when they are not needed. This cost is defined for a single time point. $FP_p = FP/(P + N)$ is the probability that a detected cooking event at a single time point did not actually occur (see Table 2). Based on Equation (14), for a given unit cost UEC_U, the total unjustified economic cost UEC_T may vary depending on the probability of non-occurrence of the detected cooking event $\left(FP_p\right)$.

Given the generally limited availability of information on actual unjustified unit costs of IAQ control, the proposed cost analysis framework employs cost ratios. Specifically, the unjustified unit cost ratio $R_U = UEN_U/UEC_U$ and the total unjustified cost ratio $R_T = UEN_T/UEC_T$ were defined. Based on Equations (13) and (14), and R_T are correlated for a particular cooking event detection system, which is characterized by its misclassification ratio $\frac{FN}{FP}$, as shown in Equation (15).

$$R_T = \frac{FN_p}{FP_p} R_U = \frac{FN}{FP} R_U \quad (15)$$

In the (R_U, R_T) coordinates, a cooking event detection system with a classification performance defined by FN/FP can be represented by a line (see Figure 3a). The linear relationship described by Equation (15) indicates that different ratios of total unjustified costs (R_T) can be achieved using a particular detection system, depending on the unit cost ratio (R_U).

For the detection system, the threshold unit cost ratio, R_{Uthr}, is defined as follows: $R_T = 1 \Leftrightarrow R_U = R_{Uthr}$. This definition implies that if $R_U = R_{Uthr}$, the detection system imposes equal total costs on the unjustified environmental and economic components $(UEN_T = UEC_T)$. Conversely, if $R_U < R_{Uthr}$, then $R_T < 1$, meaning the total cost is dominated by the economic component $(UEN_T < UEC_T)$. If $R_U > R_{Uthr}$, then $R_T > 1$, meaning the total cost is dominated by the environmental component $(UEN_T > UEC_T)$. These relationships show that a given detection system allows the total unjustified cost to be balanced in favor of either economic or environmental costs, depending on the unit cost ratio.

The proportionality constant in Equation (15) indicates that the relationship between R_T and R_U can be modified by adjusting the $\frac{FN}{FP}$ ratio. Consequently, R_{Uthr} depends on the confusion matrix of a specific classifier, which in turn is determined by the composition of the feature vector and the classifier itself. By performing a successful preselection based on classification performance measures, several candidate detection systems with satisfactorily low, yet different, FN and FP values can be identified before cost analysis. This allows flexibility in achieving a desired balance of total unjustified costs.

Each detection system has its own R_{Uthr}; therefore, for a set of candidate systems, the threshold range extends from the minimum threshold $R_{Uthrmin}$ to the maximum threshold $R_{Uthrmax}$ (see Figure 3b). If the true unit cost ratio exceeds the maximum threshold $(R_U > R_{Uthrmax})$, the total unjustified cost of IAQ control will be dominated by the environmental component $(UEN_T > UEC_T)$, regardless of the detection system applied. Conversely, if the actual unit cost ratio is below the minimum threshold $\left(R_U < R_{Uthrmin}\right)$, the total unjustified cost will be dominated by the economic component $(UEN_T < UEC_T)$.

If the actual unit cost ratio lies within the range $R_U \in (R_{Uthrmin}, {}_{Uthrmax})$, a classifier can be selected to favor either a higher total unjustified economic or environmental cost, depending on the desired outcome.

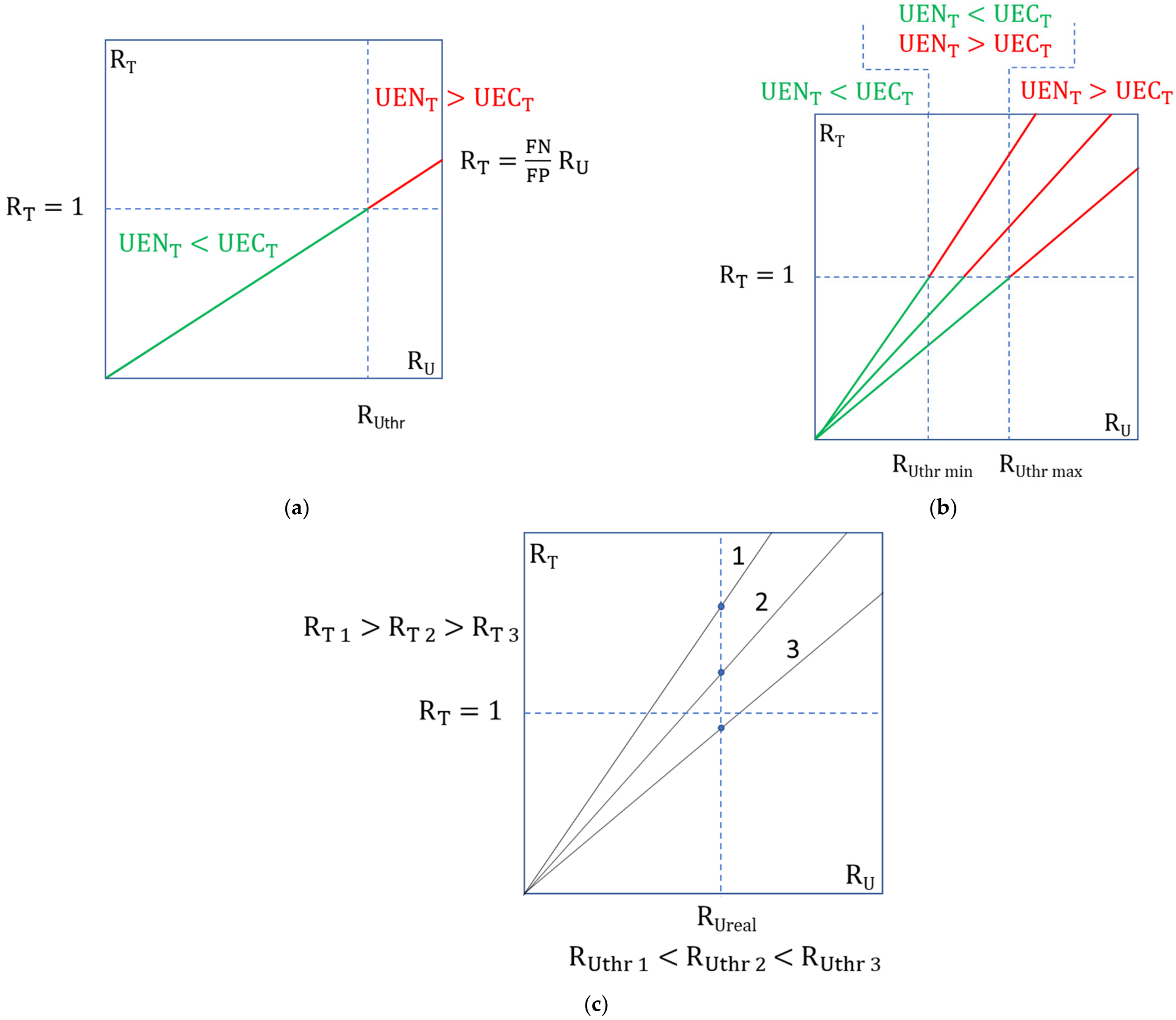

Figure 3. (**a**) Linear relationship between total unjustified costs ratio (R_T) and unit unjustified costs ratio (R_U) for a cooking event detection system, based on Equation (15). The proportionality constant ($\frac{FN}{FP}$) depends on system performance. The threshold unit cost ratio (R_{Uthr}) for the detection system is shown. It is defined as follows: $R_T = 1 \Leftrightarrow R_U = R_{Uthr}$. If $R_U < R_{Uthr}$ then $R_T < 1$ and the total unjustified environmental cost is lower ($UEN_T < UEC_T$). If $(R_U > R_{Uthrmax})$ then $R_T > 1$ and the total unjustified environmental cost is higher $UEN_T > UEC_T$. (**b**) Linear relationships between R_T and R_U for three exemplary cooking event detection systems and the associated threshold unit cost ratios. Minimum and maximum R_{Uthr} are shown for the set of detection systems. When $R_U \in (R_{Uthrmin}, R_{Uthrmax})$ the domination of total unjustified environmental or economic cost may be attained by choosing the right classifier. (**c**) For fixed $R_U = R_{Ureal}$, the contribution of UEN_T decreases (decreasing R_T) when applying detection system with increasing R_{Uthr}. Green color indicates the parts of linear relationships where $R_T < 1$ and the red color indicates the parts of linear relationships where $R_T > 1$.

The proposed cost analysis framework enables the evaluation of candidate event detection systems under a range of unit cost scenarios and allows to determine their suitability with respect to specific requirements concerning the balance between total unjustified environmental and economic costs of IAQ control.

When selecting a detection system for a specific practical application, the preferences of the system's target users are decisive. There are three possible options:

1. It is preferred to avoid unnecessary deterioration of indoor air quality (small UEN_T relative to UEC_T). This corresponds to $R_T < 1$
2. It is preferred to maintain a balance between unnecessary IAQ deterioration and unnecessary monetary expenditures (comparable UEN_T and UEC_T). This corresponds to $R_T \approx 1$
3. It is preferred to avoid unnecessary monetary expenditures (high UEN_T relative to UEC_T). This corresponds to $R_T > 1$

In a practical scenario, preferences 1, 2, or 3 have to be achieved for specified unjustified unit costs UEN_U and UEC_T, that is, for a known and fixed ratio $R_U = R_{Ureal}$.

As shown in Figure 3c, at fixed $R_{U,}$ small R_T can be achieved using detection systems with high R_{Uthr}, and big R_T can be achieved using detection systems with low R_{Uthr}. In other words, the use of classifiers with high R_{Uthr} makes it possible to prioritize the quality of indoor air, whereas the use of classifiers with low R_{Uthr} results in prioritizing the monetary aspect. When several classifiers are available which have different thresholds, to maximize achieving: option 1—select the classifier with $R_{Uthrmax}$; option 2—select the classifier with R_{Uthr} as close as possible to R_{Ureal}; and option 3—select the classifier with the $R_{Uthrmin}$.

3. Measurement Study

The measurement study was conducted in a semi-open kitchen zone of a family house. As shown in Figure 4a, the kitchen is part of an open space that also includes a dining room and a living room. The family prepares meals and cooks in the kitchen. Weekday dining primarily occurs in the kitchen, with the dining room used only occasionally. The living room is dedicated to relaxation and watching TV. The semi-open kitchen zone is the most frequently occupied area of the house due to its functionality and comfort. This type of space is representative of a common layout in modern European housing.

The measuring instrument was placed on a shelf in the passage between the kitchen and the dining room, approximately 1.5 m above the floor, as shown in Figure 4b. This location enabled monitoring the impact of cooking under real conditions, including potential interference from activities occurring in the dining and living rooms.

Measurements were conducted over 27 full days, from 27 April 2024 to 7 June 2024. Data were collected continuously with a temporal resolution of 7 s. Therefore, the total number of measurement time points was n_T = 27 days $\times$ 24 h $\times$ 3600 s/7 s $\approx$ 33 696 points. Cooking event detection was done for n time points, $n = n_T - n_{TW}$, where n_{TW} is the size of the time window utilized for feature vector formation. The considered time windows had 1, 3, 5, 7, or 9 time points.

A detailed log of activities in the open space was maintained throughout the measurement period. It had a form of written notes. The log included information on the kind of activity and its description, the time it started and ended, the number of people present in the kitchen zone, and window status.

Regarding cooking activities, the information on the food type and appliances used (cooker, oven, toaster, dishwasher, sink, stove hood) was included in the notes. Based on the notes, the following types of cooking activities involving thermal food processing took place during the study: tea and coffee making including water boiling; cooking rice, noodles, groats, pudding, cacao; cooking soup, vegetables; heating sausages, dumplings; frying fish, meat, eggs, vegetables; baking cake, pie, casserole; toasting bread; preparing toasts. Except for Easter preparation, the quantity of food prepared each time was quite stable, due to the constant number of inhabitants and their regular lifestyle. The notes were made by house occupants, supervised by one of the paper's authors.

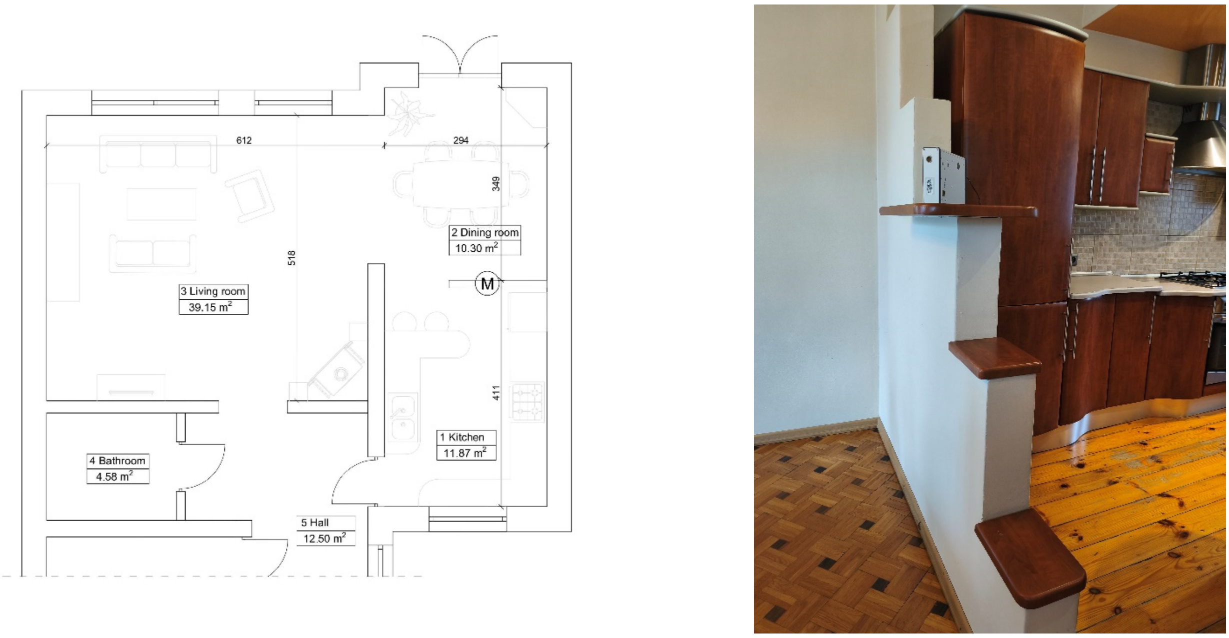

(**a**) (**b**)

Figure 4. Semi-open space, including kitchen (4.11 × 2.94 m), dining room (3.49 × 2.94 m) and living room (5.18 × 6.12 m), where the measurement study was done. (**a**) Space layout showing the location of the measurement point (M). (**b**) Sensor device at the measurement point.

The data collected during the measurement period were used to train and validate the cooking event detection system. A cooking event was defined as any activity involving thermal food processing in the kitchen. Data collected during periods of thermal food processing were labelled 'COOKING', while data recorded during periods without such activity were labelled 'NO COOKING'.

4. Results

4.1. Selection of Cooking Event Detection Systems with High Classification Performance

To develop a high-performance cooking event detection system, the dependency of classification performance on feature vector composition was analyzed. Two factors were considered: (1) the duration of measurements used to construct the feature vector, and (2) the selection of air parameters included in the feature vector. Classification performance was evaluated using the Miss Rate (MR) and False Detection Rate (FDR).

4.1.1. Selection of Measurement Data Time Window for Feature Vector Construction

The classification performance was evaluated for different time windows used to construct the feature vectors. In this analysis, each feature vector included all air parameters recorded by the sensor device: T, RH, CO_2, PM10, PM2.5, PM1, and the responses of the following sensors: TGS2600, TGS2602, PID-AH, GM102b, GM302b, GM502b, GM702b, and PMS5003 (CH_2O). The considered data collection time windows were 7, 21, 35, 49, and 63 s, corresponding to 1, 3, 5, 7, and 9 consecutive time points, respectively. Figure 5 presents the results of this analysis.

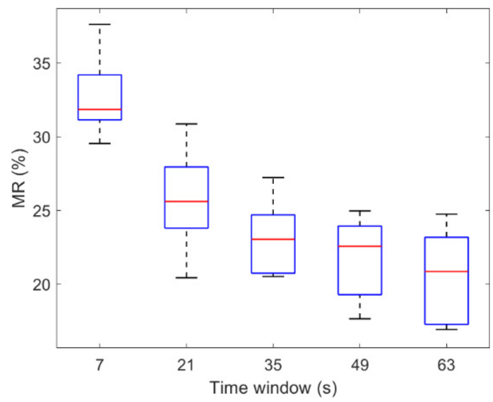

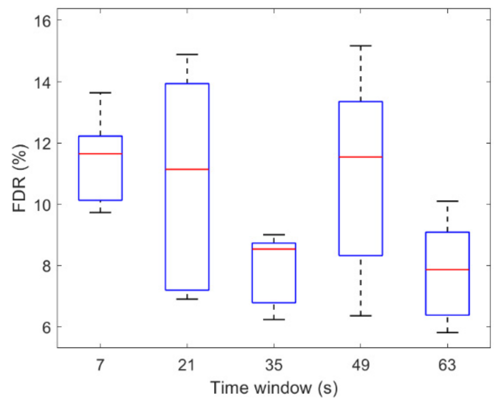

Figure 5. Results of five-fold cross-validation of DNN for cooking event detection. The DNN input data was collected in the time windows of 7, 21, 35, 49, and 63 s. The feature vector included all air parameters measured by the sensor device. They were: T, RH, CO_2, PM10, PM2.5, PM1 and the responses of the following sensors TGS2600, TGS2602, PID-AH, GM102b, GM302b, GM502b, GM702b, PMS5003(CH_2O). (**a**) Miss Rate (MR), see Equation (11). (**b**) False Detection Rate (FDR), see Equation (12).

As shown in Figure 5, across all compared time windows, the median Miss Rate (MR) ranged from 20.5% to 32.7%, and the median False Detection Rate (FDR) ranged from 7.8% to 11.4%. In all cases, FDR was lower than MR, indicating that the probability of failing to detect a cooking event that actually occurred (MR) was consistently higher than the probability of falsely detecting a cooking event when none occurred (FDR). An MR higher than the FDR indicates that the DNN was less effective at learning the pattern of the 'COOKING' class than that of the 'NO COOKING' class. This may be a consequence of the unbalanced training dataset, specifically the underrepresentation of cooking patterns. In this work, the number of feature vectors representing the 'COOKING' class was nearly 20 times smaller than the number representing the 'NO COOKING' class. In general, one may expect a cooking event detection system to exhibit a higher MR than FDR. This is because, in most real-life scenarios, cooking patterns are underrepresented in the training data. In practice, cooking takes only a limited portion of the day; therefore, fewer measurement data points are collected during cooking events than during non-cooking periods. The unbalanced structure of the training dataset reflects this fact.

Based on Figure 5, extending the data collection period from 7 to 63 s reduced MR by 12.2% and FDR by 3.6%. One-way ANOVA confirmed that the changes in MR and FDR associated with time window extension were statistically significant ($\alpha = 0.1$), with respective p-values $p = 4.61 \times 10^{-5}$ (MR) and $p = 0.076$ (FDR). Extending the data collection period beyond 9 time points did not yield further significant reductions in MR or FDR.

4.1.2. Selection of Air Parameters for Feature Vector Construction

The parameters measured by the sensor device were analyzed to determine their contribution to achieving high-performance cooking event detection. The analysis aimed to identify the parameters providing crucial information as well as those potentially redundant. Various compositions of feature vectors were considered. Throughout this analysis, the data collection time window was fixed at 63 s, based on the results presented in Section 4.1.1.

The usefulness of T, RH, and CO_2 for cooking event detection was evaluated first, as these parameters form a core set typically involved in basic assessments of indoor air quality. Classification performance was assessed when using individual air parameters (T, RH, and CO_2) or combinations thereof (T+RH, T+RH+CO_2) as inputs to the neural network.

A complementary approach was also applied: T, RH, and CO_2, or their combinations (T+RH, T+RH+CO_2), were excluded from the set of all measured parameters, and the remaining parameters were used as inputs to the network. The resulting MR and FDR values are summarized in Figure 6. The benchmarks for comparison were the MR and FDR achieved when the detection was based on all measured air parameters.

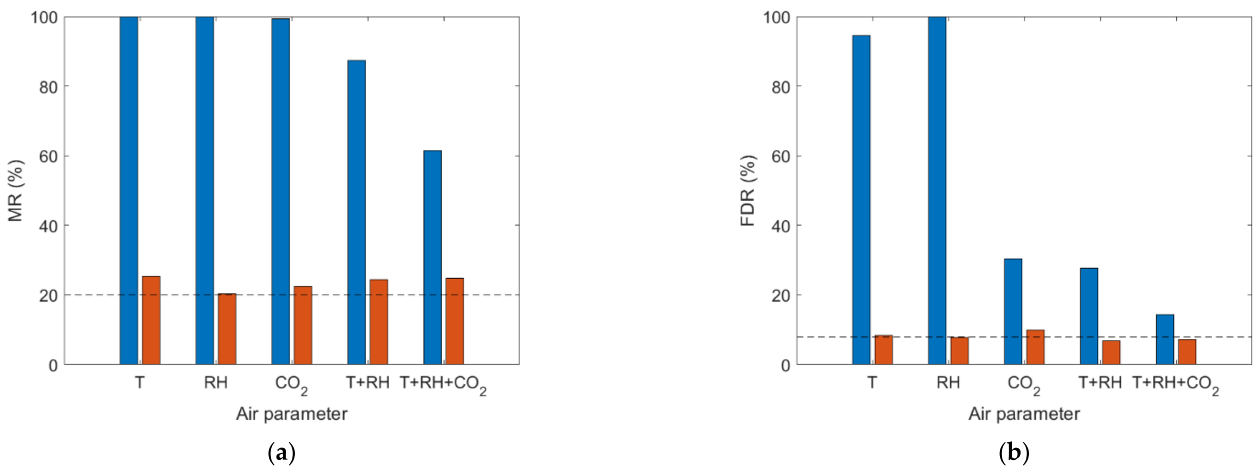

Figure 6. Dependence of cooking event detection performance on using: T, RH, and CO_2, in the feature vector. (**a**) Miss Rate (MR), see Equation (11). (**b**) False Detection Rate (FDR), see Equation (12). Blue bars in subfigures (**a**,**b**) refer to cases when the feature vector included one particular parameter or the group of parameters indicated by the respective label on the horizontal axis. Red bars in subfigures (**a**,**b**) refer to cases when the feature vector included all measured parameters except for one particular parameter, or the group of parameters indicated by the respective label on the horizontal axis. Dashed lines indicate the benchmark, i.e., the results achieved when the detection system utilized all measured air parameters.

The results indicate that effective detection of cooking events was not achievable when using T, RH, or CO_2 individually (Figure 6, blue bars for T, RH, and CO_2). The system failed to detect cooking when it occurred (Figure 6a: MR ≈ 100%) and also produced numerous false detections of cooking when it did not occur (Figure 6b: FDR = 30–100%). Detection performance improved when combining parameters (Figure 6, blue bars for T+RH and T+RH+CO_2). The best, although still unsatisfactory, results were obtained when the feature vector included all three parameters (Figure 6a: MR = 60%; Figure 6b: FDR = 15%).

Detection performance further improved when all measured parameters except T, RH, and CO_2 were used (Figure 6, red bars), with MR slightly exceeding the benchmark (by up to 5%) and FDR generally lower than the benchmark. These results suggest that while T, RH, and CO_2 together provide useful information for detecting cooking events, this information alone is insufficient for reliable detection. Moreover, other measured quantities can compensate for or replace T, RH, and CO_2 in the feature vector.

The second group of air parameters analyzed for their usefulness in cooking event detection was related to suspended particulate matter. This group included total particulate matter (PM) and its fractions (PM10, PM2.5, and PM1). Classification performance was evaluated using either total PM or individual PM fractions as inputs to the neural network. Alternatively, PM10, PM2.5, PM1, or total PM were excluded from the set of all measured parameters when constructing the feature vector. The resulting MR and FDR values are summarized in Figure 7, with reference to the respective benchmarks.

Detection of cooking events based on PM10, PM2.5, PM1, or total PM individually was largely ineffective (blue bars in Figure 7). While the probability of falsely detecting cooking when it did not occur was relatively low (Figure 7b: FDR = 24–38%), the probability of failing to detect an actual cooking event was very high (Figure 7a: MR = 92–94%).

Considering FDR (Figure 7b), total PM was a more informative parameter for cooking event detection (FDR = 24%) compared with the individual PM fractions (PM10, PM2.5, PM1; FDR = 35–38%).

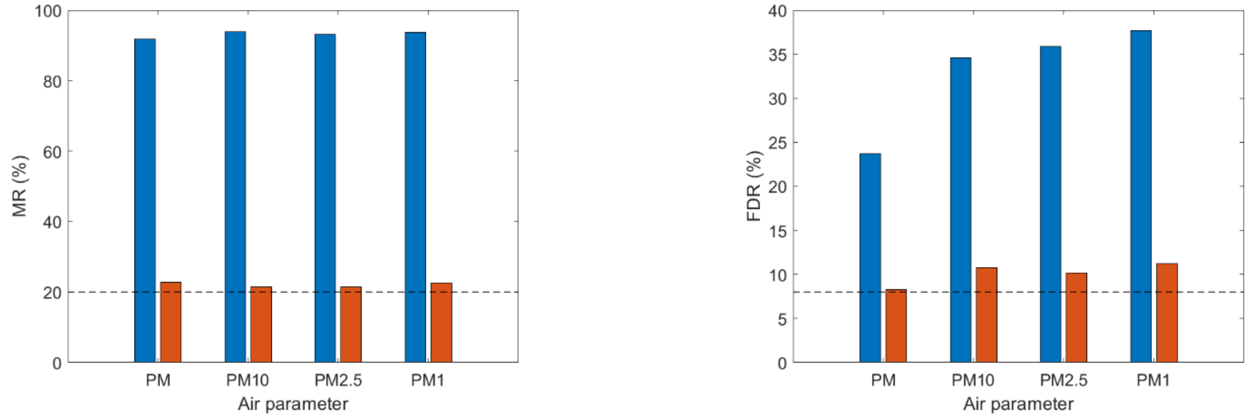

(a) (b)

Figure 7. Dependence of cooking event detection performance on using: the total content of suspended particulate matter in the air (PM) and the content of fractions: PM10, PM2.5, and PM1, in the feature vector. (**a**) Miss Rate (MR), see Equation (11). (**b**) False Detection Rate (FDR), see Equation (12). Blue bars in subfigures (**a**,**b**) refer to cases when the feature vector included one particular parameter or the group of parameters indicated by the respective label on the horizontal axis. Red bars in subfigures (**a**,**b**) refer to cases when the feature vector included all measured parameters except for one particular parameter, or the group of parameters indicated by the respective label on the horizontal axis. Dashed lines indicate the benchmark, i.e., the results achieved when the detection system utilized all measured air parameters.

Very good results were achieved when PM, PM10, PM2.5, and PM1 were removed from the set of air parameters used by the DNN (red bars in Figure 7). However, eliminating PM-related information from the network input caused both MR and FDR to increase slightly compared with the benchmark (MR by 1–2.3% and FDR by 0.3–3.2%). This indicates that particulate matter data provide distinctive information relevant to cooking event detection. Comparing the blue bars in Figures 6 and 7, total PM and PM fractions contributed more information about cooking than T, RH, or CO_2 individually. Nevertheless, both groups of parameters were insufficient for effective detection of cooking events. The MR was unacceptably high (Figures 6a and 7a, blue bars).

The third group of DNN input parameters included sensor responses to gases other than CO_2. This group comprised responses from several sensors. Specifically, VOC information was obtained from TGS2600, TGS2602, PID-AH, GM302b, GM502b, and PMS5003 (CH_2O); NO_2 information was provided by GM102b; and CO information was obtained from GM702b. Cooking event detection was attempted using individual sensor responses as well as combinations of sensors. The combinations were formed according to the following criteria: common sensor response mechanism (TGS = {TGS2600, TGS2602}; GM = {GM102b, GM302b, GM502b, GM702b}), common response mechanism but different manufacturing technologies (TGS + GM), and different response mechanisms and manufacturing technologies (TGS + GM + PID, TGS + GM + PID + PMS5003 (CH_2O)).

Additionally, the impact of excluding individual sensor responses or their groups from the full set of measured parameters during feature vector formation was evaluated. The corresponding MR and FDR values are presented in Figure 8, with reference to the respective benchmarks.

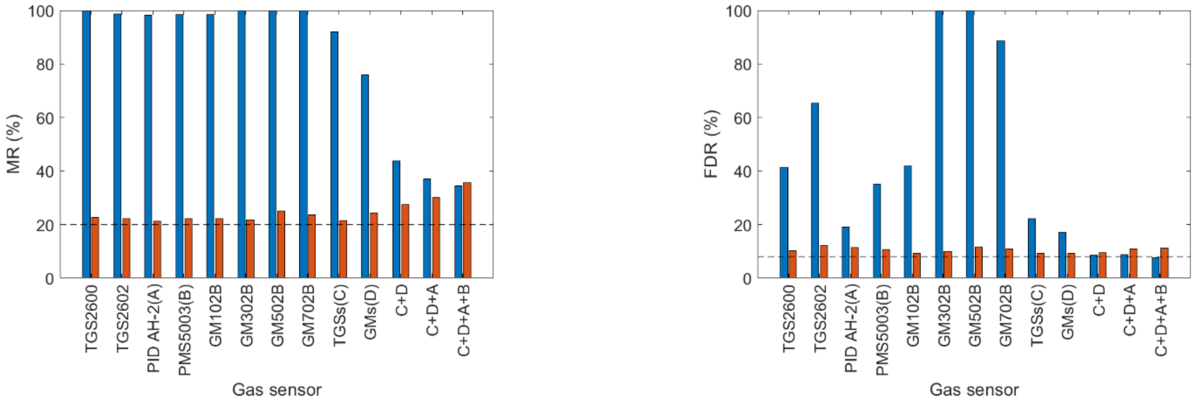

(**a**) (**b**)

Figure 8. Dependence of cooking event detection performance on using the information about the content of gases other than CO_2 in air, in the feature vector. The information about VOCs was included in the responses of sensors sensitive to these compounds: TGS2600, TGS2602, PID-AH, GM302b, GM502b, PMS5003(CH_2O). The information about NO_2 was contained in the responses of sensor GM102b. The information about CO was included in the response of sensor GM702b. (**a**) Miss Rate (MR), see Equation (11). (**b**) False Detection Rate (FDR), see Equation (12). Blue bars in subfigures (**a**,**b**) refer to cases when the feature vector included responses of one particular sensor or the group of sensors indicated by the respective label on the horizontal axis. Red bars in subfigures (**a**,**b**) refer to cases when the feature vector included all measured parameters except for responses of one particular sensor, or the group of sensors indicated by the respective label on the horizontal axis. Dashed lines indicate the benchmark, i.e., the results achieved when the detection system utilized all measured air parameters.

Detection of cooking events based on the responses of individual gas-sensitive sensors (excluding CO_2) was largely ineffective (Figure 8, blue bars). The system failed to detect actual cooking events (MR = 100%), and the fraction of detected events that did not actually occur was high (FDR = 20–100%), with strong dependence on the specific sensor. The lowest FDR (20%) was achieved using the PID sensor response.

Detection performance improved when groups of sensors were used. If the group included sensors with the same response mechanism and manufacturing technology (TGSs or GMs), FDR was low (approximately 20%), but MR remained high (around 80%). The best classification performance was obtained when the group included sensors with different response mechanisms or manufactured with different technologies (TGS+GM, TGS+GM+PID, TGS+GM+PID+PMS5003 (CH_2O)). In these cases, MR improved significantly (Figure 8a, MR = 34–44%), and FDR decreased to the benchmark level (Figure 8b). These results highlight the key role of gas sensors, particularly those responsive to VOCs, in cooking event detection. The low MR and FDR also indicate the necessity of using multiple, diverse sensors.

As shown in Figure 8, excluding gas sensor responses from the feature vector was unfavorable. Removing individual sensors caused a slight increase in MR (1–5% relative to the benchmark), while excluding groups of sensors resulted in a larger MR increase (7–15%). Regarding FDR (Figure 8b), the elimination of individual sensors or their groups caused a modest increase (up to 3%) relative to the benchmark.

A comparison of Figures 6 and 8 demonstrates that cooking event detection was most effective when using responses of multiple, diverse gas sensors. In this configuration, both MR and FDR were lower compared with detection based on other parameters, such as T, RH, CO_2, and PM combined. Thus, gas sensor responses provide a viable alternative to air parameters typically considered indicative of indoor conditions. Nevertheless, the highest classification performance was achieved when physical air parameters and gas sensor responses were combined, with the most significant improvement being MR reduction.

4.2. Best Detection Systems Regarding the Unjustified Cost of IAQ Control

The most effective cooking event detection systems were identified based on classification performance metrics, namely MR and FDR. Table 4 summarizes the performance indicators of these top detection systems, including MR, FDR, FN_p, and FP_p. In addition, the $\frac{FN_p}{FP_p}$ ratio and R_{Uthr} were presented to provide a reference for the unjustified cost analysis.

Table 4. Best systems for cooking event detection, and their performance characteristics. The following performance indicators are quoted: MR, FDR, FN_p, FP_p. In addition, the $\frac{FN_p}{FP_p}$ ratio and R_{Uthr} are presented to provide a reference for the unjustified cost analysis.

No	Air Parameters Included in the Feature Vector	MR (%)	FDR (%)	FN_p (%)	FP_p (%)	$\frac{FN_p}{FP_p}$	R_{Uthr}
1	All	20.5	8.0	1.0	0.3	3.3	0.30
2	All but T	25.4	8.3	1.3	0.3	4.3	0.23
3	All but RH	20.4	7.7	1.0	0.3	3.3	0.30
4	All but CO_2	22.5	9.9	1.1	0.4	2.8	0.36
5	All but PM10	21.5	10.8	1.1	0.5	2.2	0.45
6	All but PM2,5	21.5	10.1	1.1	0.3	3.7	0.27
7	All but PM1	22.6	11.2	1.1	0.4	2.8	0.36
8	All but PID-AH response	21.2	11.3	1.0	0.3	3.3	0.30
9	All but TGS2600 response	22.7	10.2	1.1	0.3	3.7	0.27
10	All but TGS2602 response	22.1	12.2	1.1	0.3	3.7	0.27
11	All but GM102B response	22.1	9.3	1.1	0.3	3.7	0.27
12	All but GM302B response	21.6	10.0	1.1	0.3	3.7	0.27
13	All but GM502B response	25.1	11.7	1.2	0.3	4.0	0.25
14	All but GM702B response	23.7	10.9	1.2	0.4	3.0	0.33
15	All but PMS5003 (CH_2O) response	22.3	10.6	1.1	0.3	3.7	0.27

As shown in Table 4, the best-performing detection systems utilized data collected over a 1 min period prior to detection and employed either all parameters measured by the sensor device or all parameters except one. In particular, the system that had the lowest MR and FDR (No. 3 in Table 4) utilized all air parameters except for the relative humidity of air. It was the only system that performed better than system No. 1, utilizing all measured parameters. Systems utilizing measurement data with any other air parameter excluded had MR and FDR higher than system No. 1. Based on this result, RH could be considered redundant for cooking event detection, while all other measured parameters contributed useful information. Perhaps RH did not show the distinctive behavior in the presence and absence of cooking, which made its use misleading for detection. Although water vapor content in indoor air changes during cooking, other activities could cause a similar effect, e.g., flat cleaning or weathering. Yet, our finding regarding RH redundancy for cooking event detection may be case-specific, and it shall not be generalized until similar results are obtained in other studies.

The relationship between the total unjustified costs ratio R_T and the unit unjustified costs ratio R_U was determined for the best-performing cooking event detection systems listed in Table 4, using Equation (15). The corresponding relationships are shown in Figure 9. Each detection system is represented by a linear function, with its slope determined by the respective FN_p/FP_p ratio.

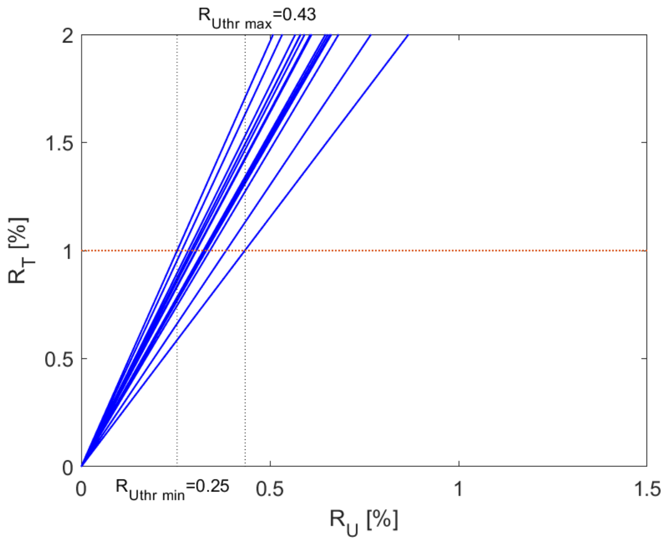

Figure 9. The linear relationship between the unjustified total costs ratio (R_T) and unjustified unit cost ratio (R_T) for the best cooking event detection systems listed in Table 4. The minimum and maximum threshold unit cost ratio for the set of classifiers has been indicated $R_{Uthrmin} = 0.25$ and $R_{Uthrmax} = 0.43$ The red dashed line indicates $R_T = 1$.

As shown in Figure 9, each detection system was capable of supporting IAQ control either with higher total unjustified environmental cost $R_T > 1$ or higher total unjustified economic cost $R_T < 1$. Yet, the possibility of achieving a particular R_T depends on the actual unit cost ratio R_{Ureal}, more specifically, on its relation to R_{Uthr} of the detection system. The flexibility in attaining a particular R_T increases when one may choose from several detection systems.

For the set of detection systems developed in this work, the minimum threshold was $R_{Uthrmin} = 0.25$, and the maximum threshold was $R_{Uthrmax} = 0.43$. Consequently, any cooking event detection system allowed IAQ control to operate with total unjustified economic costs exceeding environmental costs ($R_T < 1$) when the unit UEC was less than 25% of UEN ($R_{Ureal} < 0.25$). Conversely, IAQ control operated with total unjustified environmental costs exceeding economic costs ($R_T > 1$) when the unit UEC was more than 43% of UEN ($R_{Ureal} > 0.43$). For intermediate unit cost ratios $(0.25 \leq R_{Ureal} \leq 0.43)$, some detection systems supported a total cost balance favoring economic costs, while others shifted the balance in favor of environmental costs.

Looking for the strongest preference to IAQ, one shall choose the system featured by the biggest $R_{Uthr} = 0.43$, i.e., system No. 5 (Table 4). It offers smallest R_T irrespective of the real, unjustified unit cost ratio. Hence the share of total unjustified environmental cost is minimized. Still, for R_{Ureal} greater than 0.43, the UEN_T cost will remain higher than the economic one, even using this detection system.

The threshold R_{Uthr} depends on the $\frac{FN_p}{FPp}$ ratio, and this ratio depends on the composition of the feature vector used for cooking event detection (see Table 4). In our results, detection systems utilizing all measured parameters but one gas sensor response (Table 4, items No. 8–15, except No. 14) exhibited higher $\frac{FN_p}{FPp}$ ratios than system No. 1, using all measured parameters. This shows that removing gas sensor responses from the feature vector increased the R_{Uthr} of the detection system. As mentioned, higher R_{Uthr} implies giving preference to low unjustified environmental cost. Hence, gas sensor responses should be used for cooking event detection when giving preference to high quality indoor air. With this objective in mind, temperature was also a critical predictor, whereas CO_2, PM10, and PM1 could be considered redundant (see Table 4).

5. Discussion

Table 5 presents the cooking event detection results attained in this work together with the results of earlier studies [13,26–29]. To enable the comparison, the performance of models shown in Table 4 was expressed in terms of accuracy, precision, recall, and F1 score, which were also applied in the referred papers.

Table 5. Comparison of cooking event detection results attained in this work with the results of earlier studies [4,12–15].

Detection Model Input Data	Categories	Best Model	Accuracy * (%)	Precision * (%)	Recall * (%)	F1 Score * (%)	Reference
acoustic signals	Cooking style: "boiling (steaming)", "frying (grilling)"	Convolutional Neural Network (CNN)	90	90	90	90	[13]
acoustic signals	Cutting style: "Apple", "Banana", "Cabbage", "Carrot", "Leek", "Pepper"	Support vector machine (SVM)	96 (apple), 98 (banana), 94 (cabbage), 98 (carrot). 92 (leek), 91 (pepper)				[27]
acoustic signals	Cooking actions: "Cut", "Grill", "Other."	Gaussian mixture models (GMM)				70.53	[28]
T and RH (5 sensors in the flat and outside)	Cooking occurrence: "Cooking ", "no-cooking"	Long Short-Term Memory (LSTM) autoencoder	95	44	90		[26]
T, RH, PM2.5, TVOC, CO_2, CO, pressure, O_3, NO_2	Cooking occurrence: "Cooking", "no-cooking"	Deep learning neural network (DNN)	66.06	52.66	75.49	62.04	[29]
T, RH, CO_2, PM10, PM2.5, PM1 and the responses of the following sensors TGS2600, TGS2602, PID-AH, GM102b, GM302b, GM502b, GM702b, PMS5003(CH2O)	Cooking occurrence: "Cooking ", "no-cooking"	Deep learning neural network (DNN)	98 ± 0.01	87 ± 3.00	73 ± 3	79 ± 1	This work (Models in Table 4)

* Accuracy = $(TP + TN)/(P + N)$; Precision = $TP/(TP + FP)$; Recall = TP/P; F1score = $2TP/(2TP + FP + FN)$; see confusion matrix in Table 2 for reference.

Based on Table 5, this work presents the effective cooking event detection approach. It outperformed the most similar solution [29] in terms of accuracy (89% vs. 66%), precision (87% vs. 53%), and F1 score (97% vs. 62%), while the recall was slightly smaller (73% vs. 76%). Also, compared with [26], the only weaker performance indicator of our models was the recall (73% vs. 90%). The difficulty in attaining higher recall in this work could be related to the underrepresentation of cooking patterns in the training data set.

Developing a reliable system for detecting cooking events involves several problem-specific difficulties, which were also encountered in this study. The main challenges are data scarcity (both quantitative and qualitative) and partial temporal mismatch between the cooking activity and its reflection in indoor air parameters.

The first challenge arises because cooking in residential buildings takes only a small fraction of time daily. Previous reports indicate that people typically cook for 20–30 min per day in apartments [26]. It makes cooking event detection a rare-event problem. In principle, the dataset used for detection model building is unbalanced, containing far fewer positively labelled samples than negatively labelled ones [26]. Also in our work, such quantitative scarcity limited the generalization capability of the DNN. Also the qualitative scarcity was present. It resulted from to the finite measurement duration of approximately four weeks. Given the weekly repetition of family menus, most cooking activities were represented multiple times in the dataset; however, some dishes were prepared only once or twice, and additionally, the study included a distinctive Easter week.

The second challenge stems from the delayed impact of cooking on indoor air. The effects on air quality do not begin exactly when cooking starts, but after a short delay. Also, after cooking ends, emissions of heat and various substances continue during eating, cleaning, and other activities. An additional time is required to restore baseline indoor conditions, particularly when ventilation is weak. Previous studies reported that 1-min average PM2.5 concentrations in kitchens and living rooms peaked 1–7 min after cooking [12], with decay times potentially lasting hours depending on the species. In our study, data annotation followed the recorded start and end times of cooking; however, inspection revealed potential inconsistencies, with some data vectors reflecting cooking impact labelled as 'NO COOKING' and vice versa. Such inconsistencies impaired the DNN's ability to distinguish cooking events. Annotation of measurement data for cooking event detection remains a critical issue and is the subject of ongoing work. Nevertheless, using indoor air measurements as a source of information is attractive, as the data reflect the actual state of indoor air—an environmental component directly affected by cooking.

The results of this study emphasize that a DNN can detect cooking events based solely on the responses of gas sensors sensitive to gases other than CO_2, without information on T, RH, CO_2, or particulate matter. Detection based only on gas sensor responses achieved MR = 34.4% and FDR = 7.5%, compared with MR = 20.5% and FDR = 7.7% for the best-performing system. This confirms the key role of VOCs as markers of cooking, and the importance of information on NO_2, CO, and formaldehyde for effective detection. The study demonstrates that gas composition data have broader utility for cooking event detection than particulate matter, which is traditionally considered as linked with cooking emissions. The feasibility of collecting such data has recently increased due to the availability of compact, low-cost, and energy-efficient sensors. Regarding VOCs, it is important to employ sensors with different response mechanisms and varying sensitivities to specific substances, enabling the detection of a wide range of cooking emissions.

The presented research has its limitations. This work demonstrates that it is possible to detect cooking events in an open kitchen based on indoor air monitoring and using a DNN. Still, the system was developed and tested based on the measurement experiment performed in a semi-open kitchen for 27 days. Although this object is representative of similar objects of the same kind, the obtained results have a limited generalizability over different kinds of kitchens, cooking styles, and ventilation arrangements. The generally applicable results of the work include: the indication of air parameters to be used for cooking event detection, the recommended DNN architecture, and the estimation of achievable detection performance. Still, the developed cooking event detection system is not directly transferable to other kitchens, where cooking evokes different patterns of indoor air parameter variation. Currently, the collection of cooking impact patterns from all possible kinds of kitchens, cooking styles, ventilation solutions, etc., is not yet technically feasible. AI development could be an ally in this respect, in particular when the objects are grouped into some categories. For now, we assume that to attain an effective cooking event detection in a particular object, the detection system composed of a multi-sensor device and DNN shall be trained with the measurement data collected in that object.

A notable novelty of this work lies in linking cooking events misdetections with the unjustified IAQ control costs. A framework was developed to quantify the correspondence between IAQ control costs and faulty detections. It was shown that classification performance metrics (false positives and false negatives) determine the balance between unjustified environmental and economic costs. Moreover, FN and FP ratios can be influenced by modifying the composition of the feature vector. Consequently, the balance between UEN and UEC costs can be guided by developing a detection system with a desired FN/FP ratio (see Figure 3). In particular, gas sensor responses were found to play a major role in achieving high classification performance while keeping total unjustified environmental costs lower than economic costs (see Table 4).

The cost analysis framework proposed in this work has a general character. It can be applied in any context where detection system supports decision-making, not limited to cooking. A major limitation for its rapid adoption in environmental engineering practice is the lack of a reliable approach to estimate the unit unjustified costs. A key enabler for the broader use of the proposed approach would be developing a respective methodology.

6. Conclusions

A cooking event detection system was proposed that consists of a multi-sensor device for indoor air monitoring and a deep-learning neural network (DNN) for classification. The best-performing of the developed systems achieved a miss rate (MR) of 5.1–20.5% and a false detection rate (FDR) of 7.7–11.7%.

Cooking events were not effectively detected using basic IAQ indicators such as temperature (T), relative humidity (RH), or CO_2 concentration (best MR = 61.5% and FDR = 14.3%), nor when using particulate matter measurements alone (best MR = 91.8% and FDR = 23.7%). In contrast, the responses of sensors detecting VOCs and other non-CO_2 gases enabled acceptable detection performance (best MR = 34.4% and FDR = 7.5%). The best-performing detection system utilized all measured parameters except RH.

The presented solution is innovative in the context of sustainable housing due to the proposed detection system evaluation framework. Consideration was given to the unjustified environmental costs of IAQ control in relation to economic ones. A link between the two kinds of costs and the performance of the cooking event detection system was demonstrated.

The application prospects of the cooking event detection system are primarily associated with residential buildings. The system is intended to support the automatic control of cooking-related impacts on indoor air quality in private flats and houses. At present, the major limitations are: (1) the lack of transferability of the system between different kitchens, necessitating training with measurement data collected in the target building, and (2) the absence of a widely accepted method for estimating unit unjustified costs of IAQ control.

Future work will focus on demonstrating that the developed method is useful for (1) other activities, and (2) performed in various types of facilities, not only in residential indoor environments. It is important to determine both the degree and the scope of the method's applicability. Considerable attention will also be devoted to the selection of

https://doi.org/10.3390/su18041910

sensors that constitute the measurement matrix. The digital representation of activities associated with air quality depends on the properties of these devices and on the configuration in which they are deployed. As the effectiveness of the method depends to a large extent on data analysis, another key issue will be the identification of appropriate computational tools.

Author Contributions: Conceptualization, M.M., A.S., and J.S.; methodology, M.M., A.S., and J.S.; software, J.S.; validation, J.S., and P.D.; formal analysis, M.M.; investigation, P.D. and J.S.; resources, A.S.; data curation, P.D. and J.S.; writing—original draft preparation, M.M., A.S., J.S. and P.D.; writing—review and editing, M.M., A.S., J.S. and P.D.; visualization, M.M. and J.S.; supervision, M.M. and A.S.; project administration, M.M. and A.S.; funding acquisition, A.S. All authors have read and agreed to the published version of the manuscript.

Funding: This research was partially funded by the project POIR.04.02.00-30-A005/16-00.

Institutional Review Board Statement: Not applicable.

Informed Consent Statement: Not applicable.

Data Availability Statement: The data presented in this study are available on request from the corresponding author due to privacy concerns.

Acknowledgments: The development of prototype multi-sensor devices was financed by the project POIR.04.02.00-30-A005/16-00. The authors express gratitude to Wroclaw Centre for Networking and Supercomputing for taking care of the measurement data transmission and storage.

Conflicts of Interest: The authors declare no conflicts of interest.

References

1. Velenturf, A.P.; Purnell, P. Principles for a sustainable circular economy. *Sustain. Prod. Consum.* **2021**, *27*, 1437–1457. [CrossRef]
2. Sagadhevan, A.; Anandharajah, A.; Abdulla, F.; Yadav, A.K. Advancing smart and sustainable construction: Integrating circular economy, energy efficiency, and economic viability in the built environment. In *Mitigating Unsustainable Practices in Construction and Architecture*; González-Lezcano, R.A., Sansaniwal, S.K., Eds.; IGI Global Scientific Publishing: Hershey, PA, USA, 2026; pp. 253–276. [CrossRef]
3. Trounce, M.; Anderson, D.; Bates, L.; Bhangar, S.; Bolin, R.; Chen, W.; Chwalek, S.; Frank, S.; Hartke, J.; Kumagai, K.; et al. Paradigm shifts in indoor air quality: Insights from the 2025 Stanford forum on sustainable and healthy buildings. *Build. Environ.* **2026**, *290*, 114152. [CrossRef]
4. Kumar, S.; Sakagami, K.; Lee, H.P. Beyond sustainability: The role of regenerative design in optimizing indoor environmental quality. *Sustainability* **2025**, *17*, 2342. [CrossRef]
5. Du, Y.; Ji, Y.; Duanmu, L.; Hu, S. A case study of air infiltration for highly airtight buildings under the typical meteorological conditions of China. *Buildings* **2024**, *14*, 1585. [CrossRef]
6. Saha, T.; Saini, M.S.; Bigith, V.B. Designing for breathability: A holistic review of indoor air quality from an interior design perspective. *Multidiscip. Rev.* **2026**, *9*, e2026222. [CrossRef]
7. McCormick, E.L.; Rider, T.R. Inside out: Perceptions and realities of ambient pollution and indoor air quality in four office buildings in the United States. *Indoor Air* **2025**, *2025*, 5706819. [CrossRef]
8. Szczurek, A.; Dolega, A.; Maciejewska, M. Profile of occupant activity impact on indoor air—Method of its determination. *Energy Build.* **2018**, *158*, 1564–1575. [CrossRef]
9. Aboutorabi, R.S.S.; Yousefi, H.; Abdoos, M. A comparative analysis of the carbon footprint in green building materials: A case study of Norway. *Environ. Sci. Pollut. Res.* **2024**, *31*, 59320–59341. [CrossRef] [PubMed]
10. Li, W.; Sui, W.; Cheng, L.; Ji, Y.; Guo, Y.; Zhu, J. Quantifying seasonal demand-side flexibility in residential air conditioning under diverse control strategies. *Energy Build.* **2026**, *352*, 116764. [CrossRef]
11. Crilley, L.R.; Ditto, J.C.; Lao, M.; Zhou, Z.; Abbatt, J.P.D.; Chan, A.W.H.; VandenBoer, T.C. Commercial kitchen operations produce a diverse range of gas-phase reactive nitrogen species. *Environ. Sci. Process. Impacts* **2025**, *27*, 1517. [CrossRef]
12. Xiang, J.; Hao, J.; Austin, E.; Shirai, J.; Seto, E. Residential cooking-related PM2.5: Spatial–temporal variations under various intervention scenarios. *Build. Environ.* **2021**, *201*, 108002. [CrossRef]
13. Kim, Y.; Choi, C.-H.; Park, C.-Y.; Park, S. Examining recognition of occupants' cooking activity based on sound data using deep learning models. *Buildings* **2024**, *14*, 515. [CrossRef]

14. Navruz-Varli, S.; Bilici, S.; Ari, A.; Ertürk-Ari, P.; Ilhan, M.N.; Gaga, E.O. Organic pollutant exposure and health effects of cooking emissions on kitchen staff in food services. *Indoor Air* **2022**, *32*, e13093. [CrossRef] [PubMed]
15. Zhang, J.; Zhang, C.; Yuchi, Y.; Zhang, H.; Qiu, J.; Tang, X.; Pang, H.; Liu, X.; Hou, J.; Wang, C.; et al. Associations of solid fuel exposure and kitchen ventilation with mental disorders in rural areas. *J. Affect. Disord.* **2025**, *387*, 119522. [CrossRef] [PubMed]
16. Shen, T.; Wang, J.; Fu, Y. Exploring the relationship between home environmental characteristics and restorative effect through neural activities. *Front. Hum. Neurosci.* **2023**, *17*, 1201559. [CrossRef]
17. Liu, G.; Zou, J.; Qiao, M.; Zhu, H.; Yang, Y.; Guan, H.; Hu, S. Stress recovery at home: Effects of the indoor visual and auditory stimuli in buildings. *Build. Environ.* **2023**, *244*, 110752. [CrossRef]
18. Aksel, E.; Imamoğlu, Ç. Investigating the restorative potential of women's home environments. *J. Hous. Built Environ.* **2023**, *38*, 2793–2819. [CrossRef]
19. Zhao, J.; Nagai, Y.; Gao, W.; Shen, T.; Fan, Y. The effects of interior materials on the restorativeness of home environments. *Int. J. Environ. Res. Public Health* **2023**, *20*, 6364. [CrossRef]
20. Ha, P.P.; Warthmann, A.; van Treeck, C.; Müller, D.; Nabilou, F.; Fels, J.; Krabbe, J.; Rewitz, K.; Afamefuna, K.; Yadav, M.; et al. Indoor environmental quality in home offices. *Build. Environ.* **2026**, *287*, 113899. [CrossRef]
21. Cheng, S.; Wang, G.; Lang, J.; Wen, W.; Wang, X.; Yao, S. Characterization of volatile organic compounds from different cooking emissions. *Atmos. Environ.* **2016**, *145*, 299–307. [CrossRef]
22. Maciejewska, M.; Azizah, A.; Szczurek, A. Co-dependency of IAQ in open-kitchen restaurants. *Sensors* **2023**, *23*, 7630. [CrossRef]
23. Jiao, X.; Zhou, L.; Zhao, W.; Yuan, W.; Yang, B.; Zhang, L.; Huang, W.; Long, S.; Xu, J.; Shen, H.; et al. Cross-contamination caused by cooking fume transport. *Environ. Sci. Technol.* **2025**, *59*, 9665–9675. [CrossRef]
24. Pantelic, J.; Tang, M.; Byun, K.; Knobloch, Y.; Son, Y.J. Comparison of cooking emissions mitigation strategies. *Sci. Rep.* **2024**, *14*, 20630. [CrossRef]
25. Shang, W.; Liu, J.; Wang, C.; Li, J.; Dai, X. Smart air purifier control strategies using reinforcement learning. *Build. Environ.* **2023**, *242*, 110556. [CrossRef]
26. Khan, N.; Roy, N. Cooking event detection from thermal conditions. In Proceedings of the 2020 IEEE International Conference on Pervasive Computing and Communications Workshops (PerCom Workshops), Austin, TX, USA, 23–27 March 2020; IEEE: New York, NY, USA, 2020; pp. 1–6. [CrossRef]
27. Kojima, T.; Ijiri, T.; White, J.; Kataoka, H.; Hirabayashi, A. CogKnife: Food recognition from cutting sounds. In Proceedings of the 2016 IEEE International Conference on Multimedia & Expo Workshops (ICMEW), Seattle, WA, USA, 11–15 July 2016; IEEE: New York, NY, USA, 2016; pp. 1–6. [CrossRef]
28. Korematsu, Y.; Saito, D.; Minematsu, N. Cooking state recognition based on acoustic events. In Proceedings of the 11th Workshop on Multimedia for Cooking and Eating Activities (CEA '19), Ottawa, ON, Canada, 10 June 2019; Association for Computing Machinery: New York, NY, USA, 2019. [CrossRef]
29. Kumar, A.; O'Leary, C.; Winkless, R.; Thompson, M.; Davies, H.L.; Shaw, M.; Andrews, S.J.; Carslaw, N.; Dillon, T.J. Fingerprinting the emissions of volatile organic compounds emitted from the cooking of oils, herbs, and spices. *Environ. Sci. Process. Impacts* **2025**, *27*, 244. [CrossRef] [PubMed]
30. Gerina, F.; Massa, S.M.; Moi, F.; Reforgiato Recupero, D.; Riboni, D. Recognition of cooking activities through air quality sensor data for supporting food journaling. *Hum.-Cent. Comput. Inf. Sci.* **2020**, *10*, 27. [CrossRef]
31. Szczurek, A.; Gonstał, D.; Maciejewska, M. A multisensor IoT device for indoor monitoring. *Sensors* **2024**, *24*, 1461. [CrossRef]
32. Matilla, A.L.; Velilla, J.P.D.; Zaragoza-Benzal, A.; Ferrández, D.; Santos, P. Indoor air quality in educational buildings. *Buildings* **2023**, *13*, 2780. [CrossRef]
33. Kitchen Lighting Guide. Claremont Kitchens. Available online: https://claremontkitchens.co.uk/kitchen-lighting-guide/ (accessed on 5 January 2026).
34. Mølhave, L.; Clausen, G.; Berglund, B.; De Ceaurriz, J.; Kettrup, A.; Lindvall, T.; Maroni, M.; Pickering, A.C.; Risse, U.; Rothweiler, H. Total Volatile Organic Compounds (TVOC) in Indoor Air Quality Investigations. *Indoor Air* **1997**, *7*, 225–240. [CrossRef]
35. Lowther, S.D.; Dimitroulopoulou, S.; Foxall, K.; Shrubsole, C.; Cheek, E.; Gadeberg, B.; Sepai, O. Low-level carbon dioxide indoors. *Environments* **2021**, *8*, 125. [CrossRef]
36. World Health Organization. *WHO Guidelines for Indoor Air Quality: Selected Pollutants*; WHO: Copenhagen, Denmark, 2010. Available online: https://www.who.int/publications/i/item/9789289002134 (accessed on 5 January 2026).
37. *Standard 55-2017*; Thermal Environmental Conditions for Human Occupancy. ASHRAE: Atlanta, GA, USA, 2017. Available online: https://www.ashrae.org/file%20library/technical%20resources/standards%20and%20guidelines/standards%20addenda/55_2017_d_20200731.pdf (accessed on 5 January 2026).
38. *Standard 62.1-2016*; Ventilation for Acceptable Indoor Air Quality. ASHRAE: Atlanta, GA, USA, 2016. Available online: https://www.ashrae.org/file%20library/technical%20resources/standards%20and%20guidelines/standards%20addenda/62.1-2016/62_1_2016_s_20190726.pdf (accessed on 5 January 2026).

39. World Health Organization. *WHO Global Air Quality Guidelines*; WHO: Geneva, Switzerland, 2021. Available online: https://www.who.int/publications/i/item/9789240034228 (accessed on 5 January 2026).
40. Rumelhart, D.E.; Hinton, G.E.; Williams, R.J. Learning representations by back-propagating errors. *Nature* **1986**, *323*, 533–536. [CrossRef]
41. Hinton, G.E.; Osindero, S.; Teh, Y.W. A fast learning algorithm for deep belief nets. *Neural Comput.* **2006**, *18*, 1527–1554. [CrossRef] [PubMed]